Muhammed Alamgir, S.M. Tariqul Islam and J. A. Saju (Eds.)
ISBN: 978-984-35-4034-8

Full Paper of the WasteSafe 2023 –8th International Conference on
Integrated Solid Waste & Faecal Sludge Management
25-26 February 2023, Khulna, Bangladesh

EFFECTIVE REMOVAL OF TURBIDITY FROM TANNERY WASTEWATER BY GRAPHENE BASED NANOCOMPOSITE AS AN ADSORPTION

Kobita Roy[1], Md. Ashikur Rahaman Noyon[2], Shazneen Chowdhury[3] and Md. Elias Uddin[4]

[1,2,3,4]Department of Leather Engineering, Faculty of Mechanical Engineering, Khulna University of Engineering & Technology, Khulna 9203, Bangladesh

ABSTRACT

Excessive turbid water is aesthetically unappealing, and severely malfunctioning the photosynthesis process of aquatic ecosystem. To tackle these phenomena, this study is aiming to assess the potentiality of graphene oxide (GO)-keratin (KR) -chitosan (CS) nanocomposite adsorbent for the minimization of turbidity from tannery influent. Nanocomposites were fabricated via solution casting method while dispersibility, chemical bonding, and morphological structure of nanocomposites were analyzed through UV-Vis spectroscopy, FTIR and SEM analysis respectively. At pH 6, 2 gL^{-1} of adsorbent and 25 minutes of contact time resulted in about 88% of turbidity elimination. Furthermore, the BOD, COD, TSS, and salinity reductions are also validated for its' adsorption effectiveness. Finally, adsorption kinetics and isotherm model both justified the experimental findings ,while pseudo-second-order kinetic and Freundlich isotherm model were well suited due to the chemisorption with multilayer adsorption which ultimately responsible for the reduction of turbidity from tannery wastewater.

INTRODUCTION

The leather industry has been designated as a top-priority sector because of its potential growth and economic contribution to Bangladesh. The environmental contamination, however, prevents these sectors from complying with the requirement (Zhang et al., 2020). Leather production requires a series of batch operations where a huge amount of water is consumed and incorporates various chemical treatments to achieve the desired final leather quality. As a result, treatment of the vastness of tannery influent (20–30 m^3/ton rawhide processing) is turning into a major obstacle to upholding the discharge limit (Angelucci et al., 2017).The tannery influent is essentially highly turbid due to the presence of many contaminants, including fine organic particles of raw hides/skins, leftovers of excessive chemicals, and reagents from waste liquors (Aboubaraka et al., 2017). Thus, the direct discharge of such turbid influent prevents light penetration, reducing photosynthesis in aquatic ecosystems, and ultimately driving aquatic species towards extinction by upsetting the food chain, decreasing productivity, and impairing gill function (Solak et al., 2009; Amosa et al., 2016). Therefore, in order to address this anthropogenic digester and maintain environmental sustainability, it is imperative to guarantee a workable wastewater treatment system.

In the recent years, popular technologies have been devised to mitigate this problem including ion exchange, coagulation flocculation, membrane process, chemical precipitation, and flotation (Yusuf and Song, 2020). However, these techniques are challenging to apply in developing countries. Recently, as a cost-effective, applicable, enticing remedy, adsorption is being widely studied for its decontamination of pollutants from the environment (Payam and Arash, 2020). The utilization of nanocomposite adsorption at this point might be viewed as a sustainable water treatment technology that overcomes all current restrictions.

Graphene oxide (GO) is a highly promising nanocomposite material due to its greater specific surface area (2630 m2g-1) (Gao et al.2014).The inclusion of oxygen-based functional groups including epoxy, hydroxyl, carbonyl, and carboxyl, in addition to the surface area, render this substance unmatched as a nano adsorbent with greater pollutant removal performance (Yang, Chen et al. 2012).The assurance of electrostatic repulsion, which ensures that particles do not aggregate on GO sheets, is the driving force behind GO, it is important to note (Aboubaraka, Aboelfetoh et al. 2017).Along with GO, other biomaterials

such as chitosan, keratin, and their derivatives are used to filter out a variety of contaminants from water, such as organic and inorganic debris, oil, fat, heavy metals, and more. These biopolymers' morphological structure is also altered chemically to increase the effectiveness of adsorption. Additionally, Chitosan is inexpensive, nontoxic, pH-dependent, and extensively biodegradable (Mi et al. 2002; Ravi Kumar 2000). Therefore, change of the physicochemical qualities and stability is necessary in order to make it suitable for usage in practice by chemical modification (Srivastava et al. 2016). With this in perspective, Saha et al. 2019 fused chitosan with keratin (KR) and functionalized the adsorbent to draw charged metal ions or other contaminants from aquatic media (Saha et al 2019).GO-CS is already introduced as a viable coagulant for synthetic wastewater treatment, where it is used to eliminate turbidity as well as other impurities (Eman et al. 2016).

The aim of this study is to create an adsorbent (GO-KR-CS) from GO, keratin, and chitosan that may be used to minimize turbidity from tannery effluent . This study is the first to attempt to use nanocomposite materials like GO-KR-CS to eliminate turbidity from tannery wastewater. The nanocomposite shows remarkable effectiveness against turbid wastewater and has great promise for commercial application. The nanocomposites will work exceptionally well for the elimination of turbidity in any sort of industrial wastewater, not just tannery effluent.

MATERIALS AND METHODOLOGY

MATERIALS

Sulfuric acid, potassium permanganate, and hydrogen peroxide were acquired for the oxidation of the crystalline graphite flakes, which were then utilized to prepare GO. Reagents employed in this investigation were laboratory standard chemicals e.g., hydrochloric acid , sodium hydroxide, aluminum sulfate, sodium thiosulfate; potassium dichromate,, starch and ferrous ammonium sulfate.

PRETREATMENT OF WASTEWATER

Polythylene containers were employed to collect wastewater (sample) from several beam house operations (soaking, liming, deliming, and pickling) of the SAF Leather Industries Ltd., Jashore, Bangladesh. In this experiment, turbidity mitigation was the most prime concern by adsorption process with nanocomposites. Furthermore, some other physicochemical parameters such as pH, Turbidity, TDS, TSS, salinity, EC, BOD, COD, etc. of the treated wastewater were compared with the standard discharged level (ECR, 1997).

PREPARATION OF GO-KR-CS NANOCOMPOSITE

According to modified Hummers method, GO was synthesized by the oxidation of natural graphite flake (Uddin, Kuila et al. 2013). Keratin was prepared from sheep wool using the weight molecular destruction method. Enzymatic and alkali hydrolysis were the two phases that made up the procedure's framework (He. et al 2019). According to Toan et al. (2009), the chemical extraction approach of demineralization, deproteinization, and deacetylation was used to create chitosan from shrimp exoskeleton. T. Tanabe et al. (2002) state that keratin and chitosan were dissolved in 1:1 ratio of glacial acetic(75%) acid at 80º c and agitated for three hours at room temperature. Both solutions had been blended uniformly by ultrasonication. Chitosan and keratin were combined in an acidic environment because keratin accelerated precipitation condition in a weakly acidic environment. GO-KR-CS nanocomposites were created utilizing the simple solution mixing approach (G.Feng et al 2020). The first step of the synthesis involved dispersing prepared graphene oxide (1 g) in deionized water using ultrasonication for 1hr. To create a suitable, homogenous solution, prepared keratin and chitosan solutions were then combined dropwise and sonicated for 1.5 hours. The mixture was then transferred to a conical flask and allowed to reflux (24 hours at 80ºC) at room temperature and cooled down. To get rid of unreacted components, the residue was then collected and rinsed with de-ionized water to get rid of unreacted components. The resultant slurry was then heated once again for 72 hours at 60 °C in an oven to dry under vacuum. Finally, the residuals material was prepared as powdered form adsorbent (GO-KR-CS nanocomposite) for further use of experimentation.

CHARACTERIZATION OF GO-KR-CS NANOCOMPOSITE

The dispersibility of GO-K-CS in liquid medium (water) at room temperatures was examined using UV-Vis spectroscopy (model: UVS-2100 SCINCO). To identify the different functional groups for chemical bonding of GO-KR-CS nanocomposite, Fourier-transform infrared spectroscopy (FTIR)(model: NICOLET 6700, Perkin Elemer, USA) was conducted within the frequency range of 400-4000 cm^{-1}. The surface morphology of thermal activated adsorbents was evaluated employing SEM (JEOL JSM-6490, USA).

BATCH ADSORPTION ANALYSIS

Batch adsorption experiments on turbidity removal by GO-KR-CS nanocomposite were performed to study the adsorption efficiency and the effects of operating parameters. The removal efficiency confirmed the strength and novelty of nanocomposite throughout all the data evaluation. Finally, the turbidity (in Absorbance) of the treated samples were evaluated using UV-Vis spectrophotometer at 1100 nm wavelength. All experiments were performed threefold and the mean value and standard deviation was utilized.

Table 1 Experimental framework for batch analysis

Parameters	Range of value	Unit
pH(maintained by using 0.1 M HCl & 0.1M NaOH)	5,6,7,8,9	-
Dosage of nanocomposite	0.05,0.10,0.15,0.20,0.25	g
Contact time	15,20,25,30,35,40,45,50,60,70,80	min
Settling time	24	hrs

RESLUTS AND DISCUSSION

UV-VIS SPECTROSCOPY ANALYSIS OF NANOCOMPOSITE

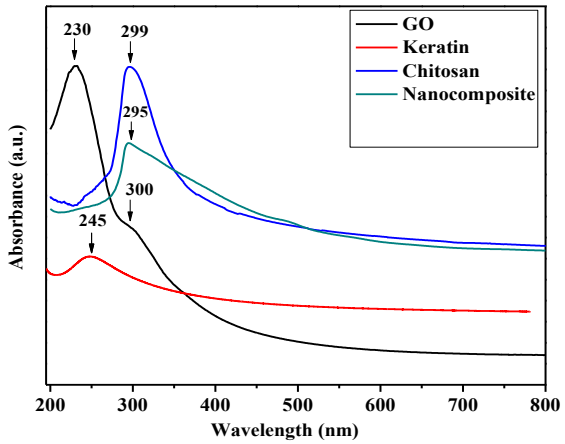

Figure 1 UV-Vis spectroscopy of pure GO, Keratin, Chitosan and Nanocomposite.

Figure 1 exhibits the UV-Vis adsorption spectra of GO, KR,CS and nanocomposite respectively. The change between intense peak highlights the presence of available functional group and conjugated bond of individual substance. The transition peak shifts in the case of nanocomposites, indicating the restoration of conjugated structures that are connected to the complex synthesis of substances (Dhayal et al., 2020).

FTIR ANALYSIS OF NANOCOMPOSITE

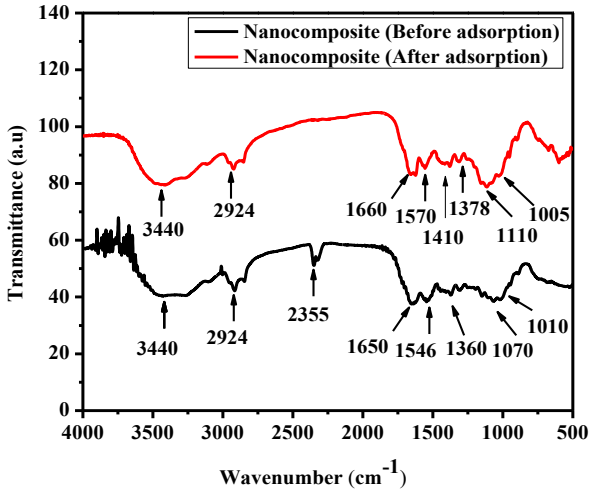

Figure 2 FT-IR analysis of Nanocomposites (Before and after adsorption).

The nanocomposite was found in spectrum at ~2924, ~2355, ~1650 ,1060 and ~1010 cm^{-1} due to the presence of C-H stretching, C=O bending and N-H bending in composite materials respectively(Fig. 2). Thus, aforementioned peaks are clearly indicating the availability of functional groups and amide linkage in nanocomposite from GO, chitosan, and keratin respectively and proving the formation of appropriate bonding. The FTIR data indicates the disappearance of functional groups, especially –OH, N-H, –CO after the adsorption process. These functional groups in the adsorbent are significant for adsorption. The –OH, –NH, –CO groups might help in bonding with the targeted materials and might be responsible for the increase the adsorbent surface area during the adsorption As a result, Adsorption capacity is influenced by the adsorbent surface's porosity and functional groups

SEM ANALYSIS OF NANOCOMPOSITE

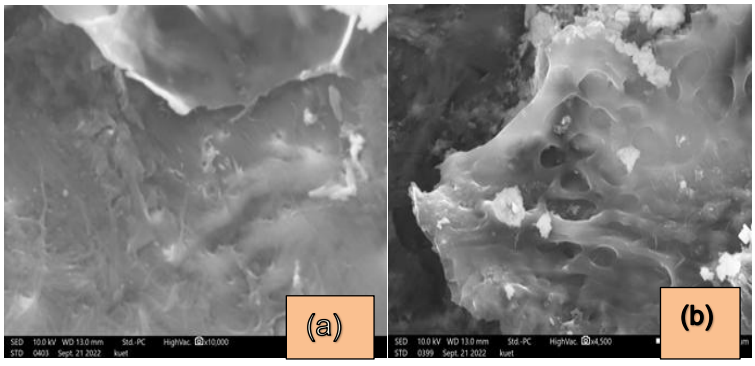

Figure 3 SEM analysis of Nanocomposites ((a) before and (b) after adsorption)

Figure 3 (a-b) presents the SEM images of GO-KR-CS nanocomposite (before and after adsorption), respectively, to understand the surface morphology, and change in structure due to adsorption process. Figure 3(a), It exhibits a multilayered smooth surface with a cloud like materials. The changes in the surface morphology of the adsorbent with a more porous surface provide a larger specific surface area to the adsorbent for the deposition of KR and CS. As a result, GO confirmed its integral structure without any agglomeration, which may have been caused by the coexistence of KR and CS in the GO matrix in 3(b) (sun et al., 2020).The difference in consistency of the pore size and surface texture are also visible through adsorption process where the suspended solid was adsorbed on the adsorbent.

EFFECT OF pH

The value of pH plays an important role for adsorption as it affects the electrostatic interaction among suspended particles as well as surface charge of adsorbent (Cardoso et al., 2011). Figure 4 depicts the effect of the initial pH of the solution on the removal of turbidity from tannery wastewater carried out at room temperature using pH in the 5.0 to 9.0 range. It can be observed that an increase in pH leads to rising turbidity removal efficiency after adsorption. In weakly acidic conditions (pH 6.0) during analysis, the highest removal percentage was attained, while in alkaline conditions (pH > 6), it drastically drops. These phenomena occurred because lower pH level influences the accession of active sites for the adsorption of effluent contaminants (Rudi et al., 2020). Additionally, flock formation and pollutant settle down slowed down at alkaline pH, which decreased the effectiveness of turbidity removal (Hayati et al., 2012).

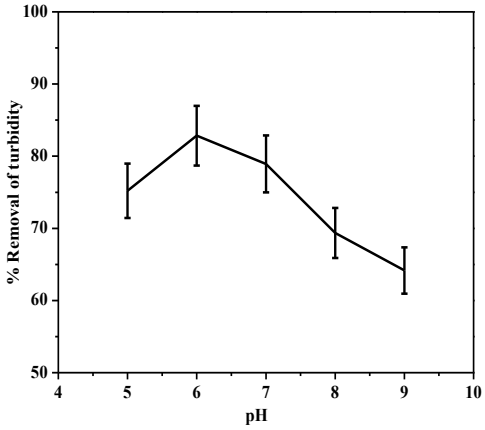

Figure 4 Effect of pH removal.

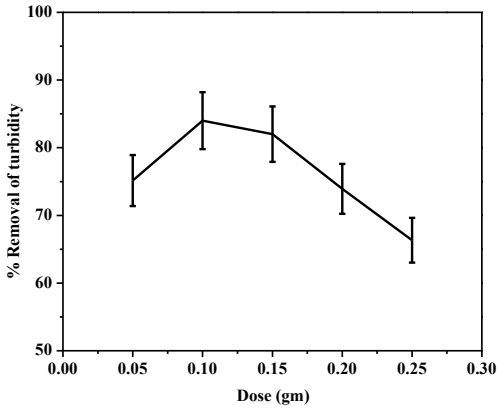

Figure 5 Effect of adsorbent dose

EFFECT OF ADSORBENT DOSE

Figure 5 shows the effect of adsorbent doses of 0.05 to 0.25 g/50 mL wastewater on adsorption capacity. This behavior relates to the available adsorption sites at lower dose which diminished even though the doses rose. At a lower dose, the amount of adsorbate is higher than the available surface area. With increasing the adsorbent dose, turbidity removal percentage increased gradually due to existence of preferable active binding sites. But it falls as shown in due to the change in the ratio of adsorbent surface area to lower concentration of adsorbate after reaching at equilibrium state. The adsorption capacity was decreased while the adsorbent dose was increased (Shoukat et al., 2017). However, process optimization is essential to prevent adsorbent overdose or settling. The highest adsorption capacity was found at a dose of 0.10 g/50 mL which was considered to be the best possible dose.

EFFECT OF CONTACT TIME

A series of adsorption analyses were performed against different contact time ranging from 20 to 70 minutes. Figure 6 represents the adsorption potential for turbidity removal against contact time of the system. It seems that the adsorption capacity increases up to 25 min and then decreases. The cause of the increase could be linked to the initial availability of external active binding sites for adsorption as observed by other researchers (Pooresmaeil et al., 2020). Adsorbate molecules were rapidly attached to the adsorbent surface via mass transfer and indicates the quick adsorption. However, after reaching equilibrium (25 min), the adsorption rate falls which might be unconventional.

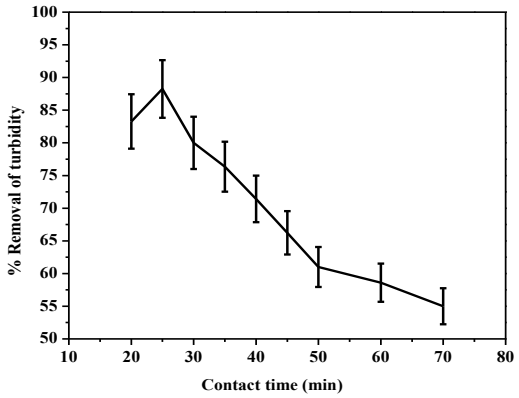

Figure 6 Effect of contact time for turbidity removal

However, the associated reasoning could be the repulsive forces of the adsorbed materials that present in the solution (Khan et al., 2017). Therefore, for this experiment 25 min was selected as the best contact time for a 50 mL sample volume.

ADSORPTION KINETICES

The reaction rate dependence on adsorption process was explored by adsorption kinetices Pseudo 1st order (PFO) and Pseudo 2nd order (PSO) kinetic models were employed to analyze and explain the adsorption kinetics. The physisorption and chemisorption are indicated in case of the fitness of adsorption process with this two model individually (Mahdavinia et al., 2016; Bai et al., 2018).The linear equation for PFO and PSO kinetic models are represented using the following equations (1), (2), respectively:

$$\ln(q_e - q_t) = \ln q_e - K_1 t \quad \text{.....(1)}$$

$$\frac{t}{q_t} = \frac{1}{K_2 q_e^2} + \frac{1}{q_e} t \quad \text{.....(2)}$$

Where: while q_e and q_t both are the values of adsorbed mass per unit adsorbent mass (mg/g) at equilibrium state and at specific time (mg/g), respectively 'K_1' (min^{-1}), 'K_2' ($gmg^{-1}min^{-1}$), 'are the rate constant of PF order, PS order, kinetic model, respectively; To evaluate the kinetics parameters, the value of log (q_e–q_t) vs. time (t), t/qt vs.t, were plotted linearly for the PFO and PSO kinetic model, respectively. The rationality of the adsorption process is determined through the calculation of coefficient value (R^2).

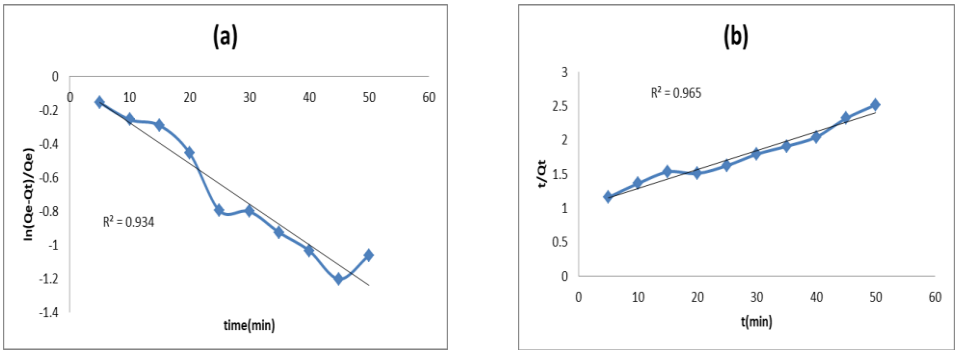

Figure 7 linear Plot of (a) pseudo-first-order and (b) second-order kinetic

Figure 7 (a, b) represent pseudo-first-order and pseudo-second-order kinetics models respectively. It is observed that, coefficient value (R^2) of the second-order kinetics is 0.965, which is higher than the coefficient value (0.934) of first-order kinetics. The accessible functional groups led to the conclusion that the adsorption mechanism was chemisorption, and there was irreversible adsorption between the contaminants and the GO-KR-CS nanocomposites.

ADSORPTION ISOTHERM

Adsorption isotherm analysis is essential to determine how interactively adsorbent and adsorbate behave in order to evaluate adsorption performance. The Langmuir, Freundlich and Temkin models were executed to explain the adsorption isotherm. Langmuir theory represents the partition mechanism of the adsorbate in solid and liquid phase following the linear isotherm model (Guo et al., 2019). To represent the multilayered adsorption theory, one of the most popular isotherms, the Freundlich model is exploited. The Temkin isotherm model specifically considers the relationship of the adsorbent-adsorbate as well as the adsorbent saturation during the process (Catherine et al., 2018). The linear equation for Langmuir, Freundlich and Temkin isotherm models are represented using the following equations (3), (4), and (5), respectively:

$$\frac{C_e}{q_e} = \frac{1}{q_m K_L} + \frac{C_e}{q_m} \quad \text{..... (3)}$$

$$\log q_e = \log K_F + \frac{1}{n} \log C_e \quad \text{.....(4)}$$

$$q_e = B_t \ln A_t + B_t \ln C_e \text{ ,Where, } B_t = \frac{RT}{b} \quad \text{.....(5)}$$

Where, q_e is the amount of adsorbed suspended solids (mg/g) at equilibrium, C_e is the concentration of aqueous solution at equilibrium state (mg/L), 'K_L' (L/mg) and 'K_F' (L/mg) are the constants of Langmuir and Freundlich adsorption isotherm, respectively; 'q_m' (mgg^{-1}) denotes the capacity of maximum adsorption; 'n' stands for the parameter of Freundlich isotherm; 'A_t' (L/g) and 'b' (J/mol) represent the constants of Temkin isotherm; 'B_t' is the constant related to the heat of adsorption; 'R' is the molar gas constant (Where, $R=8.314 Jmol\text{-}1K^{-1}$); 'T' (K) is the temperature; respectively.

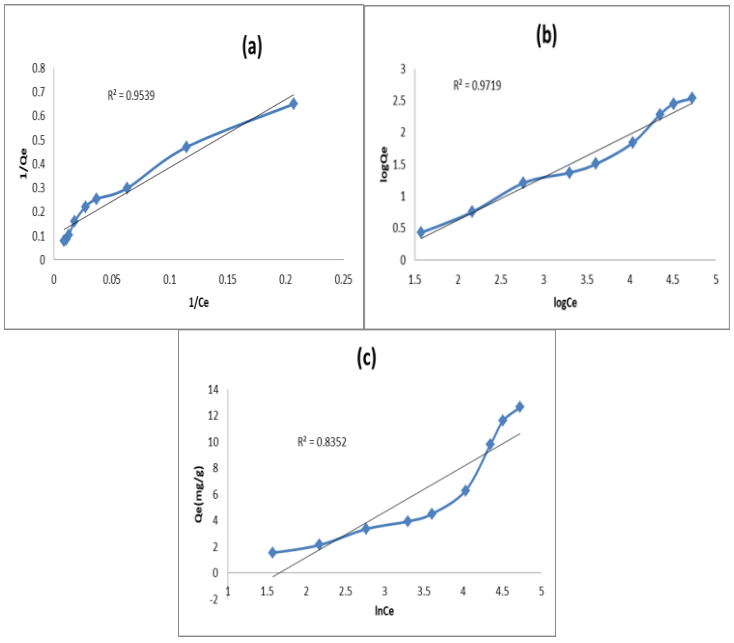

Figure 8 linear Plot of (a) Langmuir isotherm, (b) Freundlich isotherm and (c) Temkin isotherm

In this study, the correlation coefficient value of isotherms (R^2) is represented in Fig. 8. Hence, the sorption process had been more fitted with the Freundlich model R^2=0.9713 rather than Langmuir isotherm R^2=0.9531 as well as Temkin isotherm R^2=0.8352, and indicating the confirmation of multilayer adsorption into the active binding layers of GO-KR-CS nanocomposites. Here, it's worth mentioning that the aforementioned experiments were not carried out in tannery wastewater because the first time, this study is focusing the concept of turbidity removal form tannery wastewater by using GO-KR-CS nanocomposite.

Table 2 Comparison of different parameters between before and after treatment

Parameters	Unit	Raw Effluents	Treated effluent	Standard Value (ECR 97)
pH	-	8.5	6	6-9
Turbidity	(absorbance at 1100 nm	1.098)	0.129	-
Conductivity	mS	24.39	26.44	1.20
TDS	mg/L	15810	11280	2100
TSS (Total Suspended Solids)	mg/L	37190	16720	500
TS (Total Solids)	mg/L	53000	31000	-
Salinity	ppt	17.2	15.2	
DO	mg/L	4.56	6.82	4-6
BOD	mg/L	2819.51	1176	100
COD	mg/L	8962.58	2007.27	400

The experimental parameters were compared and summarized in Table 2 following a general analysis. In this investigation, the TSS, TDS, and salinity were reduced by 55, 29, and 12%, respectively, while the maximum 88% turbidity removal was obtained.

Table 3 Comparison between different studies of turbidity removal

Treatment Technology	Type of wastewater	Applied materials	Removal percentage %	References
Coagulation-flocculation	Tannery	Natural coagulant (*Citrullus lanatus* seeds)	86.7	(Sathish et al., 2018)
Flocculation	Oily wastewater	Chitosan-based flocculants (PDBC-grafted CS)	98	(Lü et al., 2019)
Adsorption	Textile	Graphene oxide	90	(de Araújo et al., 2020)
Adsorption	Tannery	Graphene Oxide-Keratin-Chitosan nanocomposite	88	This Study

This comparison confirms that the GO-KR-CS composite is extremely effective in reducing the turbidity of tannery wastewater with an 88% efficacy rate, which is higher than the conventional approach.

CONCLUSION

This study explored the fabrication and utilization of GO-KR-CS nanocomposite as adsorbent for dynamic adsorption process from tannery wastewater. The priority of the nanocomposite was analyzed by Ultraviolet-Visible spectroscopy (UV-Vis), FTIR and SEM analysis. The characterization helps to confirm chemical bonding between functional groups, dispersability and morphological analysis respectively. Adsorption efficiency study exhibits that 88% of the turbidity reduced from tannery effluent could be managed by using 2g/L GO-KR-CS based adsorbent at 6pH within 25 min. However, Different parameters play a key role in the removal of turbidity by preventing adsorbent precipitation, prolonged response times, overdose aggregation, etc. Furthermore, the BOD, COD, TSS, and salinity reductions are likewise validated by GO-KR-CS nanocomposite. The mathematical model of the adsorption kinetices and isotherm shows a highest linearity in the PSO and frendlich isotherm model , thus confirming the dependence of adsorption for turbidity removal. Additionally, this study did not take into account other studies including those on desorption and regeneration. However, further research should be done to streamline manufacturing processes, validate affordable production of the nanocomposite, sustainable disposal after use, and establish financial sustainability.

REFERENCES

Aboelfetoh, E. F., Aboubaraka, A. E., & Ebeid, E.-Z. M., 2021. Binary coagulation system (graphene oxide/chitosan) for polluted surface water treatment. *Journal of Environmental Management*, 288, 112481. doi: 10.1016/j.jenvman.2021.112481

Amosa, M. K., Jami, M. S., Alkhatib, M. a. F. R., Tajari, T., Jimat, D. N., & Owolabi, R. U., 2016. Turbidity and suspended solids removal from high-strength wastewater using high surface area adsorbent: Mechanistic pathway and statistical analysis. *Cogent Engineering, 3*(1), 1162384. https://doi.org/10.1080/23311916.2016.1162384

Ali, I., Basheer, A. A., Mbianda, X. Y., Burakov, A., Galunin, E., Burakova, I., Mkrtchyan, E., Tkachev, A., & Grachev, V., 2019. Graphene based adsorbents for remediation of noxious pollutants from wastewater. *Environment International*, 127, 160-180. https://doi.org/10.1016/j.envint.2019.03.029

Bai, R., Zhang, Y., Zhao, Z., Liao, Q., Chen, P., Zhao, P., Guo, W., Yang, F., & Li, L., 2018. Rapid and highly selective removal of lead in simulated wastewater of rare-earth industry using diglycolamic-acid functionalized magnetic chitosan adsorbents. *Journal of Industrial and Engineering Chemistry*, 59, 416-424. https://doi.org/10.1039/C9RA00010K

Cardoso, N. F., Lima, E. C., Pinto, I. S., Amavisca, C. V., Royer, B., Pinto, R. B.,... & Pereira, S. F. (2011).Application of cupuassu shell as biosorbent for the removal of textile dyes from aqueous solution.

Journal of Environmental Management, *92*(4), 1237-1247.doi. :10.1016/j.jenvman.2010.12.010

Cheng, J., Shou, Q., Wu, J., Liu, F., Dravid, V. P., & Zhang, X., 2013. Influence of component content on the capacitance of magnetite/reduced graphene oxide composite. *Journal of Electroanalytical Chemistry,* 698, 1-8.

Desta, M. B., 2013. Batch sorption experiments: Langmuir and Freundlich isotherm studies for the adsorption of textile metal ions onto teff straw (Eragrostis tef) agricultural waste. *Thermodynamics*, https://doi.org/10.1155/2013/375830

De Araújo, C. M., Oliveira do Nascimento,G. F., Bezerra da Costa, G. R., Baptisttella, A. M., Fraga, T.

J., de Assis Filho, R. B., 2020. Real textile wastewater treatment using nano graphene-based materials: optimum pH, dosage, and kinetics for colour and turbidity removal. *The Canadian Journal of Chemical Engineering*, 98(6), 1429-1440.

ECR (Environment Conservation Rules) (1997) Ministry of Environment & Forests (MoEF), Government of the People's Republic of Bangladesh

El Rouby, W., Farghali, A. A., Sadek, M., & Khalil, W. F., 2018. Fast removal of Sr (II) from water by graphene oxide and chitosan modified graphene oxide. *Journal of Inorganic and Organometallic Polymers and Materials*, 28(6), 2336-2349. https://doi.org/10.1002/adv.21665

Freundlich HMF (1906) Über die adsorption in lösungen. Z. Phys. Chem. 57, 385- 470. https://doi.org/10.1515/zpch-1907-5723

Gao, W., Xiao, P., Henkelman, G., Liechti, K. M., & Huang, R. (2014). Interfacial adhesion between graphene and silicon dioxide by density functional theory with van der Waals corrections. *Journal of Physics D: Applied Physics*, *47*(25), 255301. doi.: 10.1088/0022-3727/47/25/255301

Gong, X., Dang, G., Guo, J., Liu, Y., & Gong, Y., 2020. A sodium alginate/feather keratin composite fiber with skin-core structure as the carrier for sustained drug release*. International Journal of Biological Macromolecules,* 155, 386-392.

He, J., Xu, D., Li, J., Li, L., Li, W., Cui, W., & Liu, K., 2020. Highly efficient extraction of large molecular weight keratin from wool in a water/ethanol co-solvent. *Textile Research Journal*, 90(9-10), 1084-1093.

Kumar, M. N. R., 2000. A review of chitin and chitosan applications. *Reactive and Functional*

Polymers, 46(1), 1-27. https://doi.org/10.1016/S1381-*5*148(00)00038-9

Khan, M. U., Ahmad, S., & Al-Gahtani, H. J. (2017). Chloride-induced corrosion of steel in concrete: an overview on chloride diffusion and prediction of corrosion initiation time. *International journal of*

corrosion, *International Journal of Corrosion*, vol. ,2017,9.https://doi.org/10.1155/2017/5819202.

Langmuir I (1918) The adsorption of gases on plane surfaces of glass, mica and platinum. *J. Am. Chem.Soc*. 40(9), 1361-1403. https://doi.org/10.1021/ja02242a004

Pooresmaeil, M., & Namazi, H., 2020. Application of polysaccharide-based hydrogels for water treatments. *In Hydrogels based on natural* polymers (pp. 411-455).doi.10.1016/B978-0-12-8164211.00014-8

Rudi, N. N., Muhamad, M. S., Te Chuan, L., Alipal, J., Omar, S., Hamidon, N., Hamid, N. H. A.Sunar, N.M., Ali, R., & Harun, H., 2020. Evolution of adsorption process for manganese removal in water via agricultural waste adsorbents. *Heliyon*, 6(9), 05049.

Saha, S., Zubair, M., Khosa, M., Song, S., & Ullah, A., 2019. Keratin and chitosan biosorbent for

wastewater treatment: a review. *Journal of Polymers and the Environment*, 27(7). 1389-1403

Solak, M., Kılıç, M., Hüseyin, Y., & Şencan, A., 2009. Removal of suspended solids and turbidity from marble processing wastewaters by electrocoagulation: Comparison of electrode materials and electrode connection systems. *Journal of Hazardous Materials*, 172(1),345-352. doi10.1016/j.jhazmat.2009.07.018

Sun, C., Wang, Z., Chen, L., & Li, F., 2020. Fabrication of robust and compressive chitin and graphene oxide sponges for removal of microplastics with different functional groups. *Chemical Engineering Journal*, 393, 124796. https://doi.org/10.1016/j.cej.2020.124796

Tanabe, T., Okitsu, N., Tachibana, A., & Yamauchi, K., 2002. Preparation and characterization of keratin-chitosan composite film. Biomaterials, 23(3), 817-825. doi: 10.1016/s0142-9612(01)00187-9

Toan, N. V., 2009. Production of chitin and chitosan from partially autolyzed shrimp shell materials. *The Open Biomaterials Journal*, 1(1).

Uddin, M. E., Kim, N. H., Kuila, T., Lee, S. H., Hui, D., & Lee, J. H., 2015. Preparation of reduced graphene oxide-$NiFe_2O_4$ nanocomposites for the electrocatalytic oxidation of hydrazine. *Composites Part B: Engineering*, 79, 649-659. https://doi.org/10.1016/j.compositesb.2015.05.029

Wu, Z., Feng, W., Feng, Y., Liu, Q., Xu, X., Sekino, T., Fujii, A., & Ozaki, M., 2007. Preparation and characterization of chitosan-grafted multiwalled carbon nanotubes and their electrochemical properties. *Carbon,* 45(6), 1212-1218. http://dx.doi.org/10.1016%2Fj.carbon.2007.02.013

Yang, X., Chen, C., Li, J., Zhao, G., Ren, X., & Wang, X., 2012. Graphene oxide-iron oxide and

reduced graphene oxide-iron oxide hybrid materials for the removal of organic and inorganic pollutants.

RSC Advances, 2(23), 8821-8826. DOI: 10.1039/C4RA09541C.

Zhang, C., Lin, J., Jia, X., & Peng, B. (2016). A salt-free and chromium discharge minimizing tanning technology: the novel cleaner integrated chrome tanning process. *Journal of cleaner production*, *112*, 1055-1063. https://doi.org/10.1016/j.jclepro.2015.07.155.

.